ARM/GCSS/SPARC
TWP-ICE CRM Intercomparison Study

Ann Fridlind[1], Andrew Ackerman[1], Jon Petch[2], Paul Field[2], Adrian Hill[2], Greg McFarquhar[3], Shaocheng Xie[4], and Minghua Zhang[5]

7 January 2009

1. Introduction

The Tropical Warm Pool—International Cloud Experiment[6] (TWP-ICE) took place over and around Darwin, Australia, from January 20 through February 13, 2006. As described by *May et al*. [*2008*], TWP-ICE became "the first field program in the tropics that attempted to describe the evolution of tropical convection, including the large-scale heat, moisture, and momentum budgets at 3-hourly time resolution, while at the same time obtaining detailed observations of cloud properties and the impact of the clouds on the environment." The experiment specifically focused on the properties of outflow cirrus, aiming to document their relationship to environmental conditions. The experimental domain (Figure 1) was centered on a highly-instrumented site operated by the US Department of Energy's Atmospheric Radiation Measurement (ARM) Program[7] and a polarimetric weather radar operated by the Australian Bureau of Meteorology (BOM), surrounded by a 3-hourly sounding array and surface energy budget sites. TWP-ICE was also coordinated with the Aerosol and Chemical Transport in tropIcal conVEction (ACTIVE) Program[8] funded by the UK Natural Environment Research Council, which gathered extensive in situ measurements of environmental aerosol properties [*Vaughan et al., 2008*]. The data gathered during TWP-ICE and ACTIVE are now fully archived at the ARM Climate Research Facility[9] and the British Atmospheric Data Centre[10], respectively.

A principal motivation for TWP-ICE and the organizations that funded it is the improvement of climate forecasting skill by general circulation models (GCMs), which are hindered by inadequate representation of cloud properties and their relationship to environmental conditions [*Randall et al., 2007*]. As such, TWP-ICE aimed to provide the observations required to better understand and model tropical convection generally and cirrus outflow in particular. Because cloud properties vary on short time and space

[1] NASA Goddard Institute for Space Studies, New York, NY
[2] Met Office, Exeter, UK
[3] Department of Atmospheric Sciences, University of Illinois, Urbana, IL
[4] Lawrence Livermore National Laboratory, Livermore, CA
[5] Institute for Planetary and Terrestrial Atmospheres, Stony Brook University, Stony Brook, NY
[6] http://www.bom.gov.au/bmrc/wefor/research/twpice.htm
[7] http://www.arm.gov/sites/twp/darwin.stm
[8] http://cloudbase.phy.umist.ac.uk/field/active
[9] http://www.archive.arm.gov
[10] http://badc.nerc.ac.uk/data/active

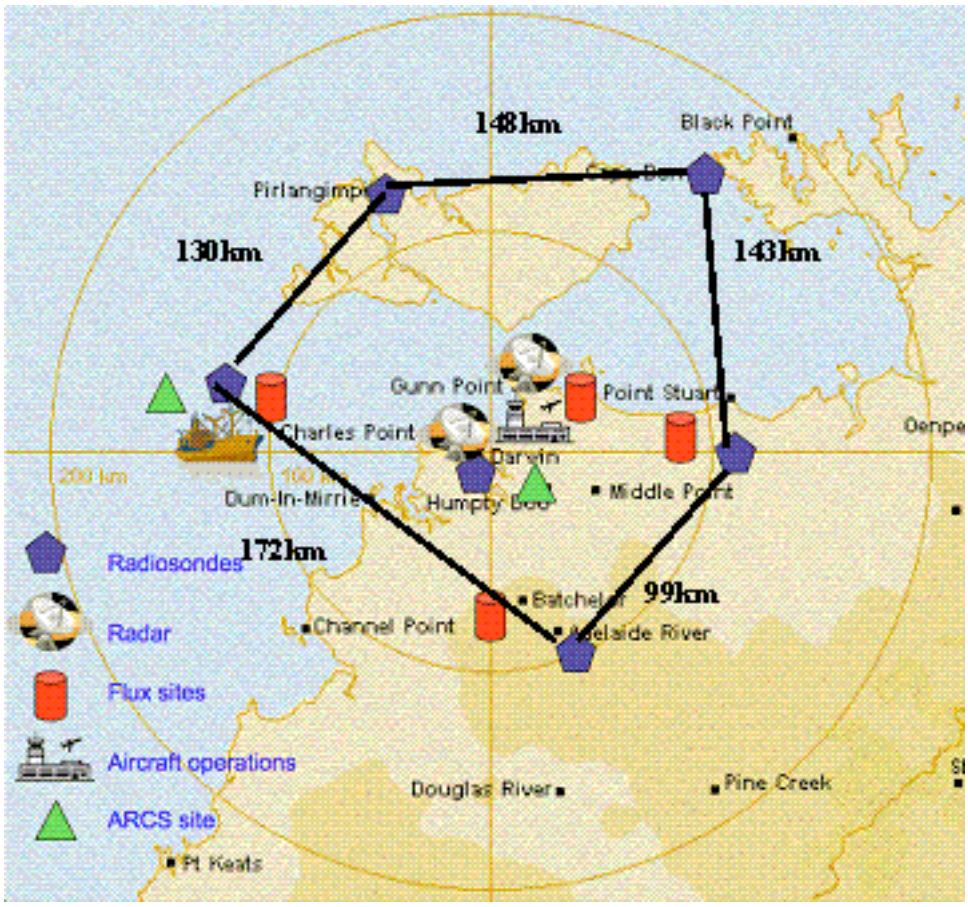

Figure 1. The TWP-ICE experimental domain as mapped for derivation of large-scale atmospheric forcing budgets. Figure courtesy of Shaocheng Xie, Lawrence Livermore National Laboratory.

scales and many fundamental aspects of their behavior remain poorly understood, an important building block for improvement of GCM cloud parameterizations has been detailed simulation of observed cloud systems with cloud-resolving models (CRMs). The GEWEX Cloud Systems Study (GCSS)[11] program has coordinated such CRM studies internationally, often based on major field experiments. Here we present the specifications for a GCSS CRM intercomparison case study based on the analysis of data gathered during the TWP-ICE and ACTIVE programs, to be performed as a joint exercise of the ARM Cloud Modeling Working Group (CMWG) and the GCSS Precipitating Cloud Systems (PCS) working group, as well as the Stratospheric Processes And their Role in Climate (SPARC)[12] program. While ARM and GCSS have previously coordinated, this will be the first joint ARM/GCSS/SPARC intercomparison, motivated by SPARC's goal of understanding the influence of tropical deep convection on water vapor concentrations and convective transport through the tropical tropopause and the

[11] http://www.gewex.org/gcss.html
[12] http://www.atmosp.physics.utoronto.ca/SPARC

unique opportunity to contribute to that understanding through high-resolution cloud modeling analysis of the TWP-ICE and ACTIVE measurements.

2. Objectives

The two principal goals of this intercomparison are to answer the following science questions: (i) what physical processes control the amount of moisture transport to the tropical upper troposphere and (ii) what physical processes control anvil cirrus cloud longevity? To answer these questions, this intercomparison will focus on the physical processes that control upper tropospheric moisture and cirrus in nature and in cloud-resolving models. Making comprehensive comparisons between observations and models is therefore a third, integral goal of this work, to be addressed first.

2.1. Objective #1: Evaluate Model Performance and Methodology

Because no previous deep convection model intercomparisons to our knowledge have focused closely on upper tropospheric moisture, we will first evaluate the performance of the models and the suitability of observations in constraining the model results. Considering that many aspects of cloud behavior remain poorly understood, especially in the upper troposphere, it is not surprising that CRMs starting from the same initial and boundary conditions may produce quite different results when it comes to anvil mass flux [e.g., *Barth et al., 2008*] or upper tropospheric moisture. Representation of anvil outflow—a final stage of complex storm system evolution—presents a challenge where models might be expected to exhibit the widest disagreement with available measurements, and measurements themselves are expected to be hardest to analyze. The first goal of this model intercomparison is to answer the following related questions:

- where do simulations and data disagree most widely?
- are data sources sufficient to evaluate model performance?
- what additional data gathering efforts should be pursued?
- is the methodology used here sufficient to answer these questions?

The approach to answering these questions will be to gather as many data sources as feasible and compare them with CRM results (Table 1). To accomplish this, it is necessary to request many diagnostics not previously included in GCSS PCS case studies. For example, ice water path retrievals are available at horizontal resolutions of order 20 km, 4 km, and less than 1 km (instantaneous vertical profile), and the last of these is currently reliable only where surface precipitation rate does not exceed circa 0.02 mm/h. Therefore, in addition to requesting that models report mean ice water path (a standard diagnostic), maximum values are requested at 20-km and 4-km resolution, and mean and maximum values are also requested at grid-scale resolution over columns where surface precipitation rate is less than 0.02 mm/h. In this manner, the data sources lead to most diagnostics requested. Measurements of each physical quantity will be evaluated against model performance as a group, such as precipitation (Figure 2, corresponding to the first measurement category in Table 1).

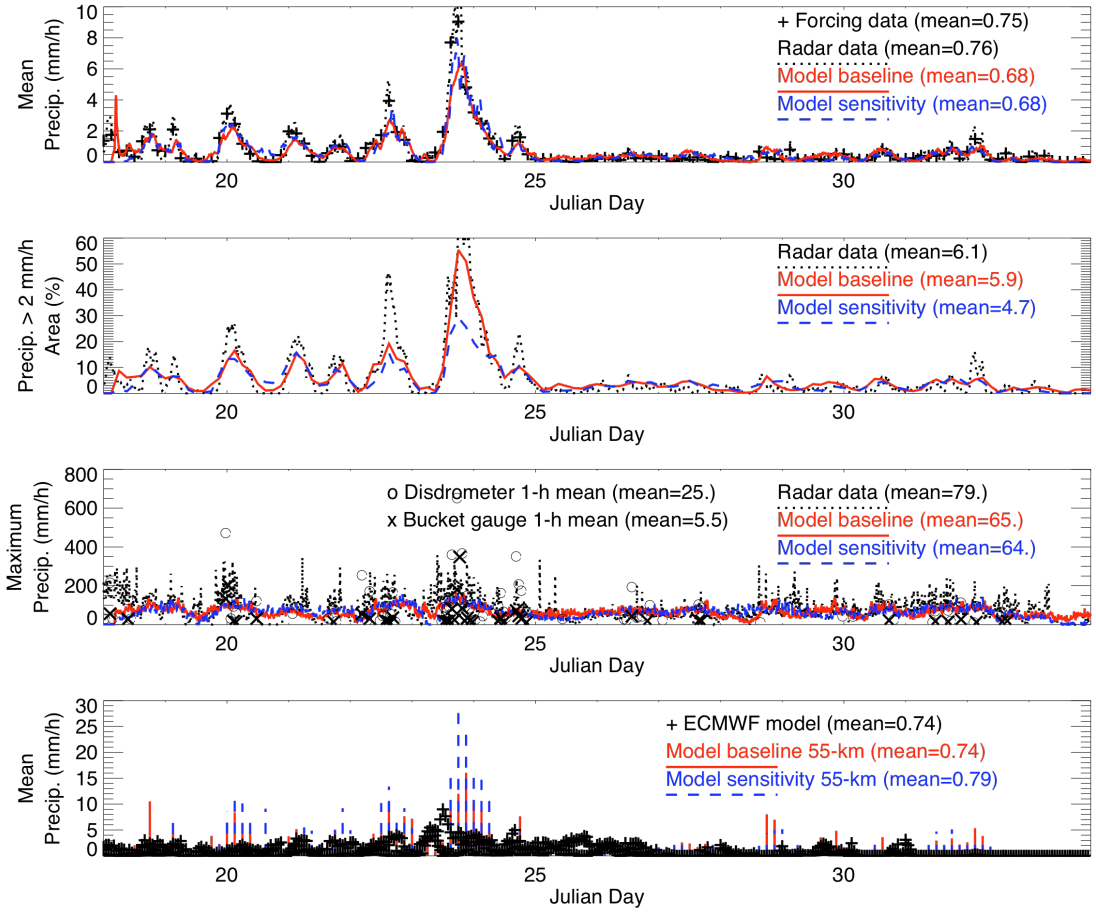

Figure 2. Comparison of requested diagnostics (described in Section 4) from example baseline and sensitivity test simulations (described in Section 3). Data courtesy of Shaocheng Xie (large-scale forcing data), Peter May (C-Pol radar data), Christopher Williams (disdrometer and bucket gauge data), and ECMWF (model).

Table 1. Data streams and model diagnostics for model evaluation, categorized by model physical variable[13]

Physical Variable	Data Set (Principal Investigator)	Model Diagnostics (Table)*
Precipitation rate	C-pol radar (May)[14]	PR2p5, PR2p5_2p5max, PR2p5_2p5F.02, .2, 2, 20 (5)
	large-scale forcing (Xie/Zhang)**	PRs (5)
	disdrometer (Williams) [15]	PRs, PRs_max (5)
	bucket gauges (Williams)	PRs, PRs_max (5)
	ECMWF model***	PRs, PRs_55max (5)

[13] http://www.giss.nasa.gov/~fridlind/twp-ice/data (examples versus data)
[14] http://www.arm.gov/instruments/instrument.php?id=cpoldar
[15] http://www.db.arm.gov/cgi-bin/IOP2/selectAftIOP.pl?iopName=twp2006twp-ice (by PI name)

Physical Variable	Data Set (Principal Investigator)	Model Diagnostics (Table)*
Liquid water mixing ratio	disdrometer (Williams)	qr, qr_max (4)
	TCPRHP ground retrieval (McFarlane/Mather/Comstock)[16]	qc_PR, qc_PRmax (4)
	ECMWF model***	qc, qc_55max (4)
Liquid water path	MWR ground retrieval (Turner)	LWP_PR, LWP_PRmax (5)
	TCPRHP ground retrieval (McFarlane/Mather/Comstock)	LWP_PR, LWP_PRmax (5)
	large-scale forcing (Xie/Zhang)**	LWP_PR, LWP_PRmax (5)
	VISST satellite retrieval (Minnis)	LWP, LWP_4max (5)
	TRMM satellite retrieval (Wentz)[17]	LWP, LWP_25max (5)
	ECMWF model***	LWP, LWP_55max (5)
Ice water mixing ratio	TCPRHP ground retrieval (McFarlane/Mather/Comstock)	qi_PR, qi_PRmax (4)
	hybrid ground-satellite retrieval (Liu)	qi, qi_20max (4)
	ECMWF model***	qi, qi_55max (4)
Ice water path	TCPRHP ground retrieval (McFarlane/Mather/Comstock)	IWP_PR, IWP_PRmax (5)
	VISST satellite retrieval (Minnis)	IWP, IWP_4max (5)
	hybrid ground-satellite retrieval (Liu)	IWP, IWP_20max (5)
	ECMWF model***	IWP, IWP_55max (5)
Total condensate mixing ratio	CSI aircraft data (McFarquhar)	qc+qi fields (3)
Water vapor	corrected radiosondes (Jakob/Hume)	qv, min, max (4) RH_RHi, min, max (4)
	aircraft in situ data (Whiteway, Hacker)[18]	qv, RH_RHi fields (3)
	large-scale forcing (Xie/Zhang)**	qv, RH_RHi (4)
	ECMWF model***	qv, 55min, 55max (5) RH_RHi, 55min, 55max (5)
Cloud base height	ARSCL ground retrieval (Clothiaux) [19]	CBH, min, max (5)
	VISST satellite retrieval (Minnis)	CBH_4 (5)
	ECMWF model***	CBH_55 (5)
Cloud top height	ARSCL ground retrieval (Clothiaux)	CTH, min, max (5)
	large-scale forcing (Xie/Zhang)**	CTH (5)
	VISST satellite retrieval (Minnis)	CTH_4 (5)
	ECMWF model***	CTH_55 (5)
Cloud cover	TSI ground instrument (Morris)[20]	CF (5)
	SFA ground retrieval (Long)	CF (5)
	MODIS satellite retrieval	CF (5)

[16] http://www.db.arm.gov/cgi-bin/PIP/viewPIP.pl?pipNo=20
[17] http://www.remss.com/tmi
[18] James Whiteway (whiteway@yorku.ca)
[19] http://science.arm.gov/vaps/arscl.stm
[20] http://www.arm.gov/instruments/instrument.php?id=tsi

Physical Variable	Data Set (Principal Investigator)	Model Diagnostics (Table)*
Radar reflectivity	C-pol radar (May)	dBZ fields (3), dBZ2p5_2p5max, 2p5F10, 30, 50 (4)
	S-band radar (Williams)	dBZ, max (4)
	disdrometer (Williams)	dBZ, max (4)
Doppler velocity	S-band radar (Williams)	DopV_min, max (4)
	disdrometer (Williams)	DopV_min, max (4)
Particle number concentration	CIP aircraft data (McFarquhar)	N_100 fields (3)
Particle projected area	CIP aircraft data (McFarquhar)	A_100 fields (3)
Particle size****	disdrometer (Williams)	MMDs_0, 0min, 0max (5)
	C-pol radar (May)	MMD2p5_2p5 (5)
	TCPRHP ground retrieval (McFarlane/Mather/Comstock)	qlRe_PR, PRmin, PRmax (4) qiRe_PR, PRmin, PRmax (4)
	VISST satellite retrieval (Minnis)	Nc and Ac fields (3) Ni and Ai fields (3)
Cloud optical thickness	TCPRHP ground retrieval (McFarlane/Mather/Comstock)	qlOD_PR, qlOD_PRmax (5) qiOD_PR, qiOD_PRmax (5)
	VISST satellite retrieval (Minnis)	OD (5)
Surface broadband radiative fluxes	TCPRHP ground retrieval (McFarlane/Mather/Comstock)	SWdn_PR, PRmin, PRmax (4) SWup_PR, PRmin, PRmax (4) LWdn,_PR PRmin, PRmax (4) LWup_PR, PRmin, PRmax (4)
	QCRAD ground data (Long)[21]	SWdn, min, max (4) SWup, min, max (4) LWdn, min, max (4) LWup, min, max (4)
	large-scale forcing (Xie/Zhang)**	SWdn, SWup, LWdn, LWup (4)
	ECMWF model***	SWdn, 55min, 55max (4) SWup, 55min, 55max (4) LWdn, 55min, 55max (4) LWup, 55min, 55max (4)
Top-of-atmosphere broadband radiative fluxes	TCPRHP ground retrieval (McFarlane/Mather/Comstock)	same as previous
	VISST satellite retrieval (Minnis)	SWup_TOA4, min, max (5) LWup_TOA4, min, max (5)
	large-scale forcing (Xie/Zhang)**	same as previous
	ECMWF model***	same as previous
Column radiative absorption	large-scale forcing (Xie/Zhang)**	same as previous
	TCPRHP ground retrieval (McFarlane/Mather/Comstock)	same as previous
	ECMWF model***	same as previous

[21] http://www.arm.gov/data/vap_process.php?id=qcrad

Physical Variable	Data Set (Principal Investigator)	Model Diagnostics (Table)*
Broadband radiative flux profiles	radiometric aircraft data (Tooman/McCoy)	SWdn, min, max (4) SWup, min, max (4) LWdn, min, max (4) LWup, min, max (4)
	TCPRHP ground retrieval (McFarlane/Mather/Comstock)	same as previous
	ECMWF model***	same as previous
Broadband radiative heating rate profiles	TCPRHP ground retrieval (McFarlane/Mather/Comstock)	SWhr_PR, PRmin, PRmax (4) LWhr_PR, PRmin, PRmax (4)
Latent heating rate profiles	radar retrieval (Schumacher)[22]	LHhr (4)
Apparent heat source and moisture sink profiles	large-scale forcing (Xie/Zhang)**	QTadv, micro, rad (4) QVadv, micro (4)
Surface sensible and latent heat fluxes	surface eddy-covariance data (Beringer)	LHflx, min, max (5) SHflx, min, max (5)
	large-scale forcing (Xie/Zhang)**	LHflx, SHflx (5)
	ECMWF model***	LHflx, SHflx (5)

*Field, profile, and scalar names are defined in Tables 3–5.
** Three-hour domain-mean values used in the variational analysis (see Section 3.2.1) are not generally independent from other data streams listed (e.g., precipitation from C-Pol, liquid water path from MWR, cloud top height from VISST, and surface broadband radiative fluxes from QCRAD).
***ECMWF model outputs are data streams available through DOE ARM that give an example of GCM-scale output.
****Particle size definitions discussed in Section 4.

2.2. Objective #2: Quantify Convective Transport to the Tropopause

After systematically evaluating model performance against available data, the second primary goal of this study is to analyze predicted convective transport to (and from) the tropopause region, including answering the following related questions:

- what are the temporal and spatial characteristics of the vertical mass transport, and how does it influence predicted water vapor mass mixing ratios in the vicinity of the tropopause?
- is ice sublimation a significant source of water vapor to any elevations in the upper troposphere (e.g., Horváth and Soden, 2008)?
- to what extent does dehydration occur in overshooting convection, and is it a significant sink of water vapor near the tropopause (e.g., Sherwood and Dessler, 2001)?
- what are the primary uncertainties in simulation results and field data?

[22] Courtney Schumacher (courtney@ariel.met.tamu.edu)

To aid this effort, four idealized tracers are included in the simulations (see Section 3.2.2) in order to efficiently evaluate transport from specific layers in the troposphere: the boundary layer, lower troposphere, mid-troposphere, and upper troposphere. Here we have used boundaries for the upper troposphere layer that are consistent with those generally adopted as boundaries of the so-called tropical tropopause layer (TTL) [e.g., *Gettelman and Forster, 2004*], namely starting where the radiative heating rate becomes positive and ending at the cold point tropopause, which during TWP-ICE persisted at circa 14–17 km. These will facilitate intercomparison of features such as predicted detrainment profile.

We also request budget profiles to allow evaluation of the sources and sinks of water vapor and hydrometeors as cloud systems evolve and dissipate (bottom of Table 4). Preliminary evaluation of these quantities led to the adoption of the single sensitivity test (see Section 3.2.1), namely the nudging of lower tropospheric thermodynamic fields, which is found to significantly influence the strength and depth of predicted convective overshooting into the TTL.

Evaluation of the predicted influence of deep convective penetrations on TTL moisture during consecutive monsoonal events observed during TWP-ICE will go hand-in-hand with model evaluation. This will be an opportunity to build on the experience of the cloud modeling community in constructing forcing data sets from field measurement arrays, driving CRM simulations in a manner consistent with those field measurements, and evaluating internal consistency of CRM predictions with all available remote-sensing and in situ measurements. During TWP-ICE, in situ data include water vapor measurements by an open-path tunable diode laser instrument up to elevations at the base of the TTL. While there are many questions that this intercomparison will be not be able to address by analyzing a single simulation and sensitivity test (e.g., regarding the relationship of microphysics treatments to CRM predictions), it is expected that general patterns will emerge from this analysis and individual CRM studies can build upon this foundation.

2.3. Objective #3: Study Anvil Cirrus Evolution

The third goal of this study is to examine anvil cirrus evolution, from formation to dissipation. Considering the several monsoon events that are observed and simulated:

- does the lag time between peak convective activity and peak anvil ice water path increase with convective event intensity (e.g., Horváth and Soden, 2008)?
- does precipitation efficiency increase with convective event intensity (e.g., Li et al., 2002)?
- in the long-lived anvil cirrus trailing the largest convective event during TWP-ICE, are observed and simulated anvil properties (e.g., ice water path, crystal sizes, fall speeds and habits) indicative of secondary ice nucleation and/or local generation of supersaturation (e.g., via radiatively induced ascent or cloud mixing)?

Tropical anvil cloud cover and precipitation efficiency have been hypothesized to play strong roles in the expected response of tropical deep convection to increasing sea

surface temperatures from greenhouse warming. GCM predictive skill may therefore depend upon the ability of models to represent processes such as anvil generation and evolution. Based on sequential observed and modeled monsoon events of increasing intensity, we will test basic relationships that have been reported among convective intensity, anvil coverage, and precipitation efficiency. We will then focus more closely on the anvil cirrus observed after the largest event. While initial anvil outflow was dominated by spherical and irregular particle habits, the aging process was accompanied by a shift to increasing numbers of bullet rosettes, indicative of subsequent vapor growth. We will investigate the sources of moisture and whether initially detrained crystals are supplemented by secondary ice nucleation.

3. Case Description

3.1. Time Period

The Darwin region experienced active monsoon conditions only during the first days of the campaign (Figure 3), culminating in the passage of a major mesoscale convective complex (MCC) directly through the center of the TWP-ICE domain on January 23 and 24, followed by suppressed conditions through February 3, and monsoon break conditions thereafter.

This first TWP-ICE model intercomparison study will consist of continuous CRM simulation of active and suppressed monsoon conditions from 0Z 18 January – 0Z 3 February (18.0-34.0 in ordinal days of 2006). Analysis will focus on model performance over several time periods:

- active monsoon conditions (19.5–25.5), comprising the first 6 days following a minimal 36 hours for model spin-up
- suppressed monsoon conditions (28–34), comprising the last 6 days of the simulated time period (avoiding the few days following 25 January when large quantities of aging anvil cirrus were advected into the domain from a mesoscale convective system located approximately 24 hours upwind)
- three 24-hour periods bounding the primary build-up and decay of consecutive monsoon events of varying strength (19.5–20.5, 22.125–23.125, and 23.5–24.5), which we refer to hereafter as events A, B, and C
- the 24-hour period of outflow cirrus evolution after event C (24.5-25.5)

Related model intercomparison studies are being separately developed for single-column models (SCMs) and limited-area models (LAMs). It is expected that the 16-day time period chosen here for CRMs will be a subset of that simulated by SCMs (which will likely include the full TWP-ICE duration through February 13) and a superset of that simulated by LAMs (which will likely comprise more detailed simulations of a few shorter time periods).

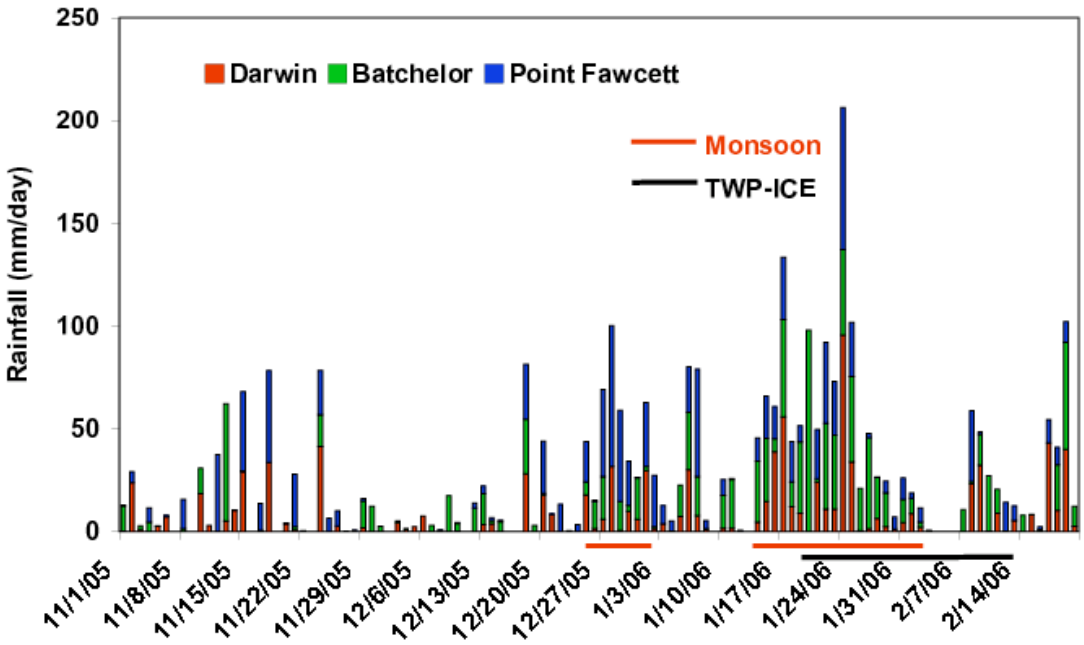

Figure 3. Cumulative rainfall at three locations in the Northern Territory during the 2005-2006 monsoon season. Figure courtesy of Lori Chappel, Australian BOM.

3.2. Model Set-Up

3.2.1. Baseline and sensitivity test

Although the TWP-ICE experimental domain contains both land and ocean regions, the low-lying land areas become saturated during the monsoon season, behaving in a manner that has been characterized as maritime in nature. To further facilitate CRM representation of relatively slowly developing and advecting monsoon features such as cold pools over the TWP-ICE region in a framework that remains as simple as possible, we adopt an idealized marine case study baseline set-up here:

- model domain footprint representative of the TWP-ICE domain size of approximately 31,000 km^2 (e.g., about 176 km east-west by 176 km north-south, or a 2-dimensional model domain representing a similar area)
- model domain height of at least 24 km
- fully-periodic horizontal boundary conditions
- uniform initial conditions at 0Z 18 January derived from mean observed profiles[23]
- random initial perturbations of –0.25 to 0.25 K in grid cells located below 500 m
- run time of 16 days, ending at 0Z 3 February

[23] http://www.giss.nasa.gov/~fridlind/twp-ice/info/txt/sound/twp_sounding.html (mean atmospheric state profiles in geometric coordinates) or http://science.arm.gov/wg/cpm/scm/scmic6/forcing_data.html (mean atmospheric state profiles in pressure coordinates)

- sea surface temperature fixed at 29°C and interactive surface fluxes
- surface albedo fixed at 0.07 in all shortwave bands
- ozone profile fixed based on sonde and OMI measurements[24]
- interactive diurnal radiation with domain centered on the Darwin ARM site (12.425°S, 130.891°E)
- horizontally uniform nudging of horizontal winds above 500 m to the mean observed profiles with a 2-hour time scale
- application of large-scale forcings derived from observations, adopted at full strength below 15 km, linearly decreasing to zero strength at 16 km[25]
- horizontally uniform nudging of mean water vapor and mean potential temperature to mean observed profiles with a 6-hour time scale, adopted at full strength above 16 km, linearly decreasing to zero strength at 15 km
- sponge layer nudging of horizontal winds and potential temperature toward their horizontal means using a nudging coefficient that increases with a $\sin^2$ vertical dependence from zero at 20 km to $(100\ s)^{-1}$ at 24 km and above

Large-scale forcings, provided as 3-hour centered-in-time domain-mean profiles with 10-mb resolution, are to be interpolated linearly in space (to model vertical grid spacing) and time (to model time step). Whereas horizontal flux divergence of potential temperature and water vapor are straightforward, large-scale vertical flux divergence of potential temperature and water vapor can be applied based on either observed or predicted profiles of potential temperature and water vapor. Here we specify that the observed mean profiles be used (rather than predicted profiles) in order to increase consistency of large-scale forcings applied to each model (because their predictions will deviate from one another). In the case of condensate and tracers, observed profiles are not available, and large-scale vertical wind (w_{LS}) will therefore need to be applied to predicted fields (f) through first-order upwinding that operates on the local vertical gradient of a field to compute the tendency as follows:

$$\text{for } w_{LS}(z+\Delta z/2) < 0,\ \partial f(z)/\partial t = -w_{LS}(z+\Delta z/2)[f(z+\Delta z)-f(z)]/\Delta z$$

$$\text{for } w_{LS}(z-\Delta z/2) > 0,\ \partial f(z)/\partial t = -w_{LS}(z-\Delta z/2)[f(z)-f(z-\Delta z)]/\Delta z$$

in which w_{LS} is staggered by half a grid cell from f. For prognostic model variables (such as total water mixing ratio) that include a component subject to a large-scale forcing that uses the observed mean profiles (water vapor in this example) and another component subject to a large-scale forcing that uses the simulated local field (condensate in this example), a hybrid approach is to be used, combining each component's appropriate forcing contribution.

---

[24] http://www.giss.nasa.gov/~fridlind/twp-ice/info/txt/ozone/twp_ozone.html

[25] http://www.giss.nasa.gov/~fridlind/twp-ice/info/txt/forc/twp_forcing.html (large-scale forcing profiles in geometric coordinates with 15-16 km scaling applied) or http://science.arm.gov/wg/cpm/scm/scmic6/forcing_data.html (large-scale forcing profiles in pressure coordinates, user needs to ensure that 15-16 km scaling is applied as specified)

The specified nudging of water vapor and potential temperature was found to be necessary in order to keep simulated environmental conditions aloft realistic, consistent with an understanding that the large-scale forcing data are insufficiently constrained by measurements above about 15 km. The use of nudging aloft allows analysis of the interaction of deep convection outflow with ambient water vapor in the tropopause region, thus serving SPARC study goals in particular. Horizontally uniform nudging of the mean predicted profiles to the mean observed profiles preserves horizontal variations.

Because it has been noted that the derived large-scale forcing profiles may tend to moisten the lower troposphere significantly more than observed, influencing the strength of convection and the depth of convective penetration, a single sensitivity test is specified in addition to the baseline simulation described above, namely:

- horizontally uniform nudging of mean water vapor and potential temperature to mean observed profiles with a 6-hour time scale, adopted at full strength above 1 km, linearly decreasing to zero strength at 500 m

In both of the simulations specified (the baseline and the sensitivity test), budget diagnostics (see Section 4) will allow analysis of the influence of nudging on the simulated fields.

3.2.2. Idealized tracers

Although extensive trace gas measurements were made by ACTIVE and TWP-ICE, it was found that concentrations in the Darwin region did not exhibit sufficient coherent, consistent vertical structure to be of use in constraining numerical simulations of vertical transport. In order to permit a first-order analysis of vertical transport among layers of the troposphere, four idealized tracers are used here, one each to represent source regions of air from the surface boundary layer (0–250 m), lower troposphere (2–4 km), mid-troposphere (4–6 km), and upper troposphere (14–17 km, which matches the canonical definition of the TTL well during the simulation dates). Because the simulation time (weeks) is very long relative to typical timescales of vertical convective transport (hours), we adopt the following treatment (identical for both baseline and sensitivity test simulations):

- initialize each tracer mixing ratio to 1.0 in its source layer (0–250 m, 2–4 km, 4–6 km, and 14–17 km) and 0.0 elsewhere
- subject tracers to advection, mixing, and large-scale vertical motion (as typically done)
- decay each tracer everywhere with a 6-hour e-folding time (i.e., apply a constant loss rate $dC/dt = -C/\tau$, where C is the local tracer mixing ratio and $\tau = 6$ hours)
- reset each tracer to 1.0 in its source layer at the end of each time step

This procedure permits efficient analysis of convective transport over long simulation times. For instance, mean boundary layer tracer concentration profiles can be compared after events A, B, and C during each simulation to evaluate relative strength of transport to and from the TTL.

3.2.3. Aerosols

While thermodynamic factors play a dominant role in the determination of condensate mass concentration in many convective clouds, cloud particle number concentration and size distribution fields are also influenced by ambient aerosol properties in a manner that remains poorly understood in the case of deep convection. Furthermore, the properties of natural aerosols over the depth of the troposphere are difficult to represent concisely because composition, morphology, and number size distribution all vary. The approach we take here is similar to that adopted by the deep convection CRM intercomparison conducted by *Barth et al*. [*2007*]. Namely, we provide a relatively simplified representation of aerosol properties based on available measurements (Figure 4), but do not specify how models should make use of it since they may employ varying degrees of complexity to represent aerosol properties.

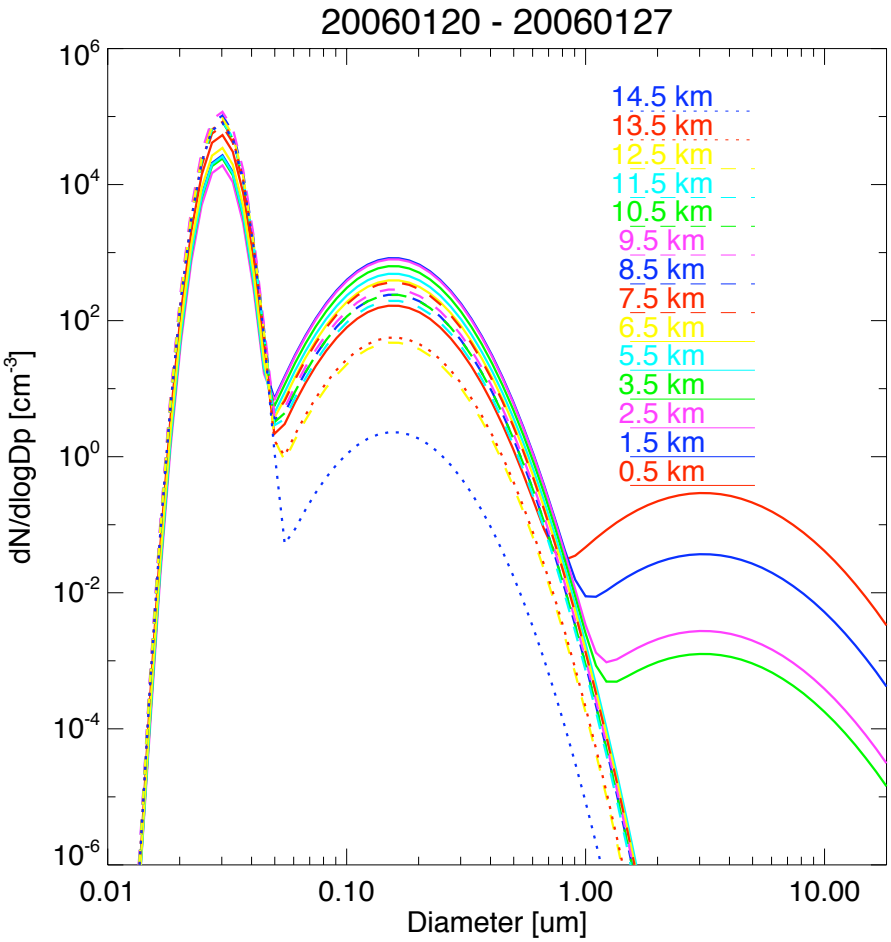

Figure 4. Aerosol number size distributions between the surface and 14 km, based on ACTIVE in situ measurements as described in Section 2.2.3.

To start, median profiles of aerosol number concentration are derived for three size cuts (dry diameter greater than 0.01, 0.04, and 0.5 μm) based on data gathered from condensation particle counter (CPC), cloud and aerosol spectrometer (CAS), and forward-scattering spectrometer probe (FSSP, dry sizes estimated where relative

humidity between 75% and 95% by assuming growth factors for ammonium sulfate) on the Egret and Dornier aircraft from the surface to circa 15 km (data courtesy of Martin Gallagher and Paul Williams, University of Manchester). Size distribution parameters for three lognormal modes (modal diameters of 0.03, 0.18, and 4.4 μm, and standard deviations of 1.12, 1.45, and 1.8) are then adopted as typical of active monsoon conditions during the 2005–2006 Darwin monsoon based on *Allen et al.* [*2008*]. Finally, a number concentration in each mode is calculated from the median profiles for each of the three size cuts[26].

Aerosol composition in the lower troposphere was dominated by sulfate, ammonium and organic species [*Allen et al., 2008*]. During the active monsoon, this composition can be approximated as a mixture of 80% by mass ammonium sulfate and 20% organics. During the inactive monsoon, it can be approximated as 70% ammonium bisulfate and 30% organics. If a uniform composition is assumed, 75% ammonium sulfate and 25% organics by mass is recommended.

4. Results to Submit

Model results are requested from 19.5–34 Julian (skipping the first 36 hours for model spin-up). Requested files fall into the three general categories (see Table 2):

- instantaneous 3-D fields at 3-hour intervals (Table 3)
- instantaneous 1-D profiles at 10-minute intervals (Table 4)
- instantaneous scalar quantities at 10-minute intervals (Table 5)

All files must be submitted in netCDF format with specified variable names and dimensions (Tables 2–5) in order to be analyzed. The output files must conform with version 1.3 of the NetCDF Climate and Forecast Metadata Conventions[27], which will facilitate the development of automated software to plot model results through a web interface. A brief summary of CF 1.3 requirements and recommendations is available online[28], as is a web interface to a compliance checker[29]. Submitted output should use the dimension and variable names and provide all the metadata that appears in the provided output templates[30], which conform to the CF 1.3 requirements (thus, if the templates are faithfully mimicked, there is no need for participants to learn anything about CF 1.3). Variables that are not submitted should be omitted from submitted files in order to conserve disk space. For variables that are submitted, missing or blank fields (e.g., minimum cloud base in a clear column) should be filled with the value defined by each netCDF variable's_FillValue attribute. Upload instructions will be provided at the ARM CMWG TWP-ICE intercomparison home page[31].

---

[26] http://www.giss.nasa.gov/~fridlind/twp-ice/info/txt/aer/twp_aerosol.html
[27] http://cf-pcmdi.llnl.gov/documents/cf-conventions/1.3
[28] http://cf-pcmdi.llnl.gov/conformance/requirements-and-recommendations/1.3/
[29] http://puma.nerc.ac.uk/cgi-bin/cf-checker.pl
[30] http://www.giss.nasa.gov/~fridlind/twp-ice/spec/templates/index.html
[31] http://science.arm.gov/wg/cpm/scm/scmic6

A few conventions are adopted throughout Tables 3–5. First, all condensate species are grouped into three categories: cloud water, rain water, and ice. All ice and mixed-phase particles are placed in the ice category. Models that carry a single size distribution for all liquid (e.g., size-resolved microphysics) should divide the distribution into cloud water and rain water based on particle size: radius ≤ 40 μm in the cloud water category and radius > 40 μm in the rain category.

Second, all diagnostics are requested at the model's own vertical and horizontal grid resolution unless otherwise specified. When horizontal resolutions larger than a given model's horizontal grid scale are specified (e.g., 2.5 km, 4 km, 20 km, or 55 km), they should be treated by dividing the model domain into as many sub-domains as possible at the requested resolution (e.g., three 55-km sub-domains fit into a 192-km domain), and the remaining model domain should be neglected (placement of the subdomains is not important, as long as they do not overlap). The requested diagnostic should then be reported over the available sub-domains. No vertical resolution changes should ever be made (only horizontal and only when requested).

Third, cloud boundaries are defined as locations where total cloud liquid and ice mass (excluding rain) exceed 10^{-6} kg kg^{-1} at the specified resolution. This applies to diagnostics that include cloud base, cloud height, cloud fraction, and mass flux.

Fourth, condensate optical depths are requested at a wavelength of 0.65 μm, or, alternatively, at any wavelength or wavelength band in the range of 0.3–0.7 μm. Aside, as noted in Table 5, when the total domain mean optical depth is called for, column values over 100 should be set to 100 prior to averaging over the domain (in order to allow comparison with satellite retrievals).

Finally, two types of size information are requested: effective radius and mass mean diameter. All effective radius values should be expressed as $3Q/(4\varrho A)$, where Q is the relevant condensate mass mixing ratio, A is the projected area, and ϱ is the condensate mass density (1.0 g cm^{-3} should be used for both liquid and ice groups, regardless of actual density). To avoid numerical problems, effective radius values should be reported only where the relevant condensate mass exceeds 10^{-6} kg kg^{-1}. (Please note that unlike the condensate mass that defines cloud boundaries, which excludes rain, effective radius diagnostics may include rain water.) Grid cell averages over multiple particle groups should be made by first totaling Q and A, and then, if the total Q > 10^{-6} kg kg^{-1}, calculating the quotient. Similarly, mean values over multiple grid cells should be made by first totaling all relevant Q and A values, and then, if the total Q > 10^{-6} kg kg^{-1}, calculating the quotient. The mass mean diameter is the fourth moment of the distribution divided by the third moment. For a Marshall-Palmer rain distribution, for instance, the mass mean diameter requested in Table 5 would be a factor of 8/3 times the 2.5-km value of effective radius requested in Table 4.

Aside, potential temperature is defined here with a reference pressure of 1000 mb. Water vapor and hydrometeor budget profiles requested in K d^{-1} should be converted from mass mixing ratio per unit time by multiplying by the latent heat of evaporation and dividing by the specific heat of air at constant pressure.

Table 2. Summary of outputs, files, and naming conventions

Type	Interval	Naming Convention*	Files/Run
3-D fields	3-hour	MODEL.VARIABLE.nc	19
Vertical profiles	10-minute	MODEL.profiles.nc	1
Scalars	10-minute	MODEL.scalars.nc	1

*'MODEL' is a unique character label to be chosen by the participant. 'VARIABLE' is one of the 19 variable names listed in the first column of Table 3 (e.g., T, u, v, etc.).

Table 3. 3-D fields at 3-hour intervals (one file per field)

Name	Units	Description
Dimensions		
time	—	number of output times = 117
xc	—	number of east-west columns
xb	—	number of east-west column boundaries = xc + 1
yc	—	number of north-south columns
yb	—	number of north-south column boundaries = yc + 1
zc	—	number of vertical layers
zb	—	number of vertical layer boundaries (including surface and top of model) = zc + 1
Axes (dimension of same name as axis)		
time	h	hours since 2006-01-18 00:00:00.0 UTC
xc	m	location of east-west column centers
xb	m	location of east-west column boundaries
yc	m	location of north-south column centers
yb	m	location of north-south column boundaries
zc	m	height above sea surface of layer centers
zb	m	height above sea surface of layer boundaries
Variables (dimensions are time; xc or xb; yc or yb; zc or zb)		
T	K	air temperature
u	$m\ s^{-1}$	eastward wind
v	$m\ s^{-1}$	northward wind
w	$m\ s^{-1}$	vertical wind (positive upward)
qv	$kg\ kg^{-1}$	water vapor mass mixing ratio
qc	$kg\ kg^{-1}$	cloud water mass mixing ratio
qr	$kg\ kg^{-1}$	rain water mass mixing ratio
qi	$kg\ kg^{-1}$	ice mass mixing ratio
Nc	L^{-1}	number concentration of cloud drops where cloud water mass mixing ratio > 10^{-6} $kg\ kg^{-1}$
Nr	L^{-1}	number concentration of rain drops where rain water mass mixing ratio > 10^{-6} $kg\ kg^{-1}$
Ni	L^{-1}	number concentration of ice particles where ice mass mixing ratio > 10^{-6} $kg\ kg^{-1}$
N_100	L^{-1}	total number concentration of cloud, rain and ice particles with maximum dimension exceeding 100 μm where total condensate mass mixing ratio > 10^{-6} $kg\ kg^{-1}$
Ac	$\mu m^2\ L^{-1}$	projected area of cloud drops, per unit volume of air, where cloud water mass mixing ratio > 10^{-6} $kg\ kg^{-1}$
Ar	$\mu m^2\ L^{-1}$	projected area of rain drops, per unit volume of air, where rain water mass mixing ratio > 10^{-6} $kg\ kg^{-1}$

Name	Units	Description
Ai	$\mu m^2\ L^{-1}$	projected area of ice particles, per unit volume of air, where ice mass mixing ratio > 10^{-6} kg kg^{-1}
A_100	$\mu m^2\ L^{-1}$	total projected area of cloud, rain and ice particles with maximum dimension exceeding 100 μm, per unit volume of air, where total condensate mass mixing ratio > 10^{-6} kg kg^{-1}
RH_RHi	—	water vapor mixing ratio divided by saturation mixing ratio (with respect to water where T ≥ 273.15, ice where T < 273.15 K)
dBZ	dBZ	Rayleigh-regime radar reflectivity
DopV	m s^{-1}	Rayleigh-regime reflectivity-weighted Doppler velocity (positive downward) where reflectivity > –10 dBZ

Table 4. Profiles at 10-minute intervals (one file)

Name	Units	Description
Dimensions		
time	—	number of output times= 2089
zc	—	number of vertical layers
zb	—	number of vertical layer boundaries (including surface and top of model) = zc + 1
Axes (dimension of same name as axis)		
time	h	hours since 2006-01-18 00:00:00.0 UTC
zc	m	height above sea surface of layer centers
zb	m	height above sea surface of layer boundaries
Variables (dimensions are time; zc or zb)		
P	Pa	mean air pressure
T	K	mean air temperature
rhobar_air	kg m^{-3}	reference density of air
u	m s^{-1}	mean eastward wind
v	m s^{-1}	mean northward wind
w_min	m s^{-1}	minimum vertical wind (maximum downdraft)
w_max	m s^{-1}	+ maximum (maximum updraft)
RH_RHi	—	mean water vapor mass mixing ratio divided by saturation mass mixing ratio (with respect to water in grid cells where T ≥ 273.15, ice where T < 273.15 K)
RH_RHi_min	—	+ minimum
RH_RHi_max	—	+ maximum
RH_RHi_55min	—	minimum water vapor mass mixing ratio divided by saturation mass mixing ratio (with respect to water in grid cells where T ≥ 273.15, ice where T < 273.15 K) at 55-km resolution
RH_RHi_55max	—	+ maximum
qv	kg kg^{-1}	mean water vapor mass mixing ratio
qv_min	kg kg^{-1}	+ minimum
qv_max	kg kg^{-1}	+ maximum
qv_55min	kg kg^{-1}	minimum water vapor mass mixing ratio at 55-km resolution
qv_55max	kg kg^{-1}	+ maximum

Name	Units	Description
qc	kg kg^{-1}	mean cloud water mass mixing ratio
qc_max	kg kg^{-1}	+ maximum
qc_PR	kg kg^{-1}	mean cloud water mass mixing ratio of columns where surface precipitation rate < 0.02 mm h^{-1}
qc_PRmax	kg kg^{-1}	+ maximum
qc_55max	kg kg^{-1}	maximum cloud water mass mixing ratio at 55-km resolution
qr	kg kg^{-1}	mean rain water mass mixing ratio
qr_max	kg kg^{-1}	+ maximum
qr_55max	kg kg^{-1}	maximum rain water mass mixing ratio at 55-km resolution
qi	kg kg^{-1}	mean ice mass mixing ratio
qi_max	kg kg^{-1}	+ maximum
qi_PR	kg kg^{-1}	mean ice mass mixing ratio of columns where surface precipitation rate < 0.02 mm h^{-1}
qi_PRmax	kg kg^{-1}	+ maximum
qi_20max	kg kg^{-1}	maximum ice mass mixing ratio at 20-km resolution
qi_55max	kg kg^{-1}	maximum ice mass mixing ratio at 55-km resolution
CF	—	fractional area covered by cloudy grid cells
CF_up0	—	fractional area covered by cloudy grid cells in which vertical wind > 0 m s^{-1}
CF_up5	—	fractional area covered by cloudy grid cells in which vertical wind > 5 m s^{-1}
BCF_up	—	fractional area covered by buoyant cloudy grid cells in which vertical wind > 0 m s^{-1}
MF_up0	kg m^{-2} s^{-1}	mass flux averaged over cloudy grid cells in which vertical wind > 0 m s^{-1}
MF_up5	kg m^{-2} s^{-1}	mass flux averaged over cloudy grid cells in which vertical wind > 5 m s^{-1}
BMF_up	kg m^{-2} s^{-1}	mass flux averaged over buoyant cloudy grid cells in which vertical wind > 0 m s^{-1}
dBZ_2p5max	dBZ	maximum Rayleigh-regime radar reflectivity at 2.5-km resolution
dBZ_2p5F10	—	fractional area of Rayleigh-regime radar reflectivity at 2.5-km resolution > 10 dBZ
dBZ_2p5F30	—	and > 30 dBZ
dBZ_2p5F50	—	and > 50 dBZ
DopV	m s^{-1}	mean Rayleigh-regime reflectivity-weighted Doppler velocity (positive downward) over grid cells where reflectivity > –10 dBZ
DopV_min	m s^{-1}	+ minimum
DopV_max	m s^{-1}	+ maximum
trBL	—	mean boundary-layer tracer mixing ratio
trBL_min	—	+ minimum
trBL_max	—	+ maximum
trLT	—	mean lower-troposphere tracer mixing ratio
trLT_min	—	+ minimum
trLT_max	—	+ maximum

Name	Units	Description
trMT	—	mean mid-troposphere tracer mixing ratio
trMT_min	—	+ minimum
trMT_max	—	+ maximum
trUT	—	mean upper-troposphere tracer mixing ratio
trUT_min	—	+ minimum
trUT_max	—	+ maximum
SWdn	W m^{-2}	mean shortwave downwelling radiative flux
SWdn_min	W m^{-2}	+ minimum
SWdn_max	W m^{-2}	+ maximum
SWdn_55min	W m^{-2}	minimum shortwave downwelling radiative flux at 55-km resolution
SWdn_55max	W m^{-2}	+ maximum
SWdn_PR	W m^{-2}	mean shortwave down radiative flux of columns where surface precipitation rate < 0.02 mm h^{-1}
SWdn_PRmin	W m^{-2}	+ minimum
SWdn_PRmax	W m^{-2}	+ maximum
SWup	W m^{-2}	mean shortwave upwelling radiative flux
SWup_min	W m^{-2}	+ minimum
SWup_max	W m^{-2}	+ maximum
SWup_55min	W m^{-2}	minimum shortwave upwelling radiative flux at 55-km resolution
SWup_55max	W m^{-2}	+ maximum
SWup_PR	W m^{-2}	mean shortwave upwelling radiative flux of columns where surface precipitation rate < 0.02 mm h^{-1}
SWup_PRmin	W m^{-2}	+ minimum
SWup_PRmax	W m^{-2}	+ maximum
LWdn	W m^{-2}	mean longwave downwelling radiative flux
LWdn_min	W m^{-2}	+ minimum
LWdn_max	W m^{-2}	+ maximum
LWdn_55min	W m^{-2}	minimum longwave downwelling radiative flux at 55-km resolution
LWdn_55max	W m^{-2}	+ maximum
LWdn_PR	W m^{-2}	mean longwave downwelling radiative flux of columns where surface precipitation rate < 0.02 mm h^{-1}
LWdn_PRmin	W m^{-2}	+ minimum
LWdn_PRmax	W m^{-2}	+ maximum
LWup	W m^{-2}	mean longwave upwelling radiative flux
LWup_min	W m^{-2}	+ minimum
LWup_max	W m^{-2}	+ maximum
LWup_55min	W m^{-2}	minimum longwave upwelling radiative flux at 55-km resolution
LWup_55max	W m^{-2}	+ maximum
LWup_PR	W m^{-2}	mean longwave upwelling radiative flux of columns where surface precipitation rate < 0.02 mm h^{-1}
LWup_PRmin	W m^{-2}	+ minimum
LWup_PRmax	W m^{-2}	+ maximum
SWhr	K d^{-1}	mean shortwave broadband heating rate
SWhr_min	K d^{-1}	+ minimum

Name	Units	Description
SWhr_max	K d^{-1}	+ maximum
SWhr_PR	K d^{-1}	mean shortwave broadband heating rate of columns where surface precipitation rate < 0.02 mm h^{-1}
SWhr_PRmin	K d^{-1}	+ minimum
SWhr_PRmax	K d^{-1}	+ maximum
LWhr	K d^{-1}	mean longwave broadband heating rate
LWhr_min	K d^{-1}	+ minimum
LWhr_max	K d^{-1}	+ maximum
LWhr_PR	K d^{-1}	mean longwave broadband heating rate of columns where surface precipitation rate < 0.02 mm h^{-1}
LWhr_PRmin	K d^{-1}	+ minimum
LWhr_PRmax	K d^{-1}	+ maximum
LHhr	K d^{-1}	mean latent heating rate
QVact	K d^{-1}	mean water vapor tendency
QVhorLS	K d^{-1}	mean large-scale water vapor horizontal flux convergence
QVverLS	K d^{-1}	mean large-scale water vapor vertical flux convergence
QVadv	K d^{-1}	mean water vapor resolved and subgrid-scale vertical flux convergence (excluding large-scale)
QVmicro	K d^{-1}	mean water vapor tendency from exchange with hydrometeors
QVnudge	K d^{-1}	mean water vapor tendency from nudging
QHact	K d^{-1}	mean hydrometeor tendency
QHverLS	K d^{-1}	mean large-scale hydrometeor vertical flux convergence
QHadv	K d^{-1}	mean hydrometeor resolved and subgrid-scale vertical flux convergence (excluding large-scale)
QHsed	K d^{-1}	mean sedimentation flux convergence of hydrometeors
QTact	K d^{-1}	mean potential temperature tendency
QThorLS	K d^{-1}	mean large-scale potential temperature horizontal flux convergence
QTverLS	K d^{-1}	mean large-scale potential temperature vertical flux convergence
QTadv	K d^{-1}	mean potential temperature resolved and subgrid-scale vertical flux convergence (excluding large-scale)
QTmicro	K d^{-1}	mean potential temperature tendency from microphysics
QTrad	K d^{-1}	mean potential temperature tendency from radiative heating
QTnudge	K d^{-1}	mean potential temperature tendency from nudging

Table 5. Scalars at 10-minute intervals (one file)

Name	Units	Description
Dimension		
time	—	number of output times = 2089
Axis (dimension of same name as axis)		
time	h	hours since 2006-01-18 00:00:00.0 UTC
Variables (all have single dimension, time)		
LWP	g m^{-2}	mean liquid water path
LWP_max	g m^{-2}	+ maximum

Name	Units	Description
LWP_PR	g m^{-2}	mean liquid water path where surface precipitation rate < 0.02 mm h^{-1}
LWP_PRmax	g m^{-2}	+ maximum
LWP_4max	g m^{-2}	maximum liquid water path at 4-km resolution
LWP_25max	g m^{-2}	maximum liquid water path at 25-km resolution
LWP_55max	g m^{-2}	maximum liquid water path at 55-km resolution
IWP	g m^{-2}	mean ice water path
IWP_max	g m^{-2}	+ maximum
IWP_PR	g m^{-2}	mean ice water path where surface precipitation rate < 0.02 mm h^{-1}
IWP_PRmax	g m^{-2}	+ maximum
IWP_4max	g m^{-2}	maximum ice water path at 4-km resolution
IWP_20max	g m^{-2}	maximum ice water path at 20-km resolution
IWP_55max	g m^{-2}	maximum ice water path at 55-km resolution
PRs	kg m^{-2} s^{-1}	mean surface precipitation rate
PRs_max	kg m^{-2} s^{-1}	maximum surface precipitation rate
PRs_55max	kg m^{-2} s^{-1}	maximum surface precipitation rate at 55-km resolution
PR2p5	kg m^{-2} s^{-1}	mean precipitation rate at 2.5-km
PR2p5_2p5max	kg m^{-2} s^{-1}	maximum precipitation rate at 2.5-km elevation and resolution
PR2p5_2p5F0p02	—	fractional area where precipitation rate at 2.5-km elevation and resolution > 0.02 mm h^{-1}
PR2p5_2p5F0p2	—	and > 0.2 mm h^{-1}
PR2p5_2p5F2	—	and > 2 mm h^{-1}
PR2p5_2p5F20	—	and > 20 mm h^{-1}
CBH	km	mean cloud base height in cloudy columns
CBH_min	km	+ minimum
CBH_max	km	+ maximum
CBH_4	km	mean cloud base height in cloudy columns at 4-km resolution
CBH_55	km	mean cloud base height in cloudy columns at 55-km resolution
CTH	km	mean cloud top height in cloudy columns
CTH_min	km	+ minimum
CTH_max	km	+ maximum
CTH_4	km	mean cloud top height in cloudy columns at 4-km resolution
CTH_55	km	mean cloud top height in cloudy columns at 55-km resolution
CF	—	fractional area covered by cloudy columns
MMDs_0	mm	mean mass mean diameter of raindrops at the surface where reflectivity > 0 dBZ
MMDs_0min	mm	+ minimum
MMDs_0max	mm	+ maximum
MMD2p5_25	mm	mean mass mean diameter of raindrops at 2.5 km where reflectivity > 25 dBZ
qlOD	—	mean optical thickness of cloud water and rain
qlOD_max	—	+ maximum

Name	Units	Description
qlOD_PR	—	mean optical thickness of cloud water and rain in columns where surface precipitation rate < 0.02 mm h^{-1}
qlOD_PRmax	—	+ maximum
qiOD	—	mean optical thickness of ice
qiOD_max	—	+ maximum
qiOD_PR	—	mean optical thickness of ice in columns where surface precipitation rate < 0.02 mm h^{-1}
qiOD_PRmax	—	+ maximum
OD	—	mean optical thickness of cloud water, rain and ice, with column values of optical thickness > 129 set to 129
OD_min	—	+ minimum
OD_max	—	+ maximum (129 if greater than 129)
SWdnTOA	W m^{-2}	mean shortwave downwelling flux at top-of-atmosphere
SWupTOA	W m^{-2}	mean shortwave upwelling flux at top-of-atmosphere
SWupTOA_4min	W m^{-2}	minimum shortwave upwelling flux at top-of-atmosphere at 4-km resolution
SWupTOA_4max	W m^{-2}	+ maximum
LWupTOA	W m^{-2}	mean longwave upwelling flux at top-of-atmosphere
LWupTOA_4min	W m^{-2}	+minimum longwave upwelling flux at top-of-atmosphere at 4-km resolution
LWupTOA_4max	W m^{-2}	+ maximum
LHflx	W m^{-2}	mean latent heat flux at surface (positive upward and excluding precipitation)
LHflx_min	W m^{-2}	+ minimum
LHflx_max	W m^{-2}	+ maximum
SHflx	W m^{-2}	mean sensible heat flux at surface (positive upward)
SHflx_min	W m^{-2}	+ minimum
SHflx_max	W m^{-2}	+ maximum

5. Schedule and Expected Outcomes

5.1. Deadlines

Preliminary results are requested by 1 March 2009. Final results are required by 1 July 2009.

5.2. Publications

It is expected that at least three modeling groups will submit results that will be contribute to papers addressing the objectives outlined in Sections 2.1–2.3. Submitted results will be included in these papers and participants included as co-authors.

5.3. Archive of Model Results and Analyzed Measurements

There are two ways it is planned to allow efficient future use of the results generated by this intercomparison study after it is completed. First, as described above, 3-D fields from each of the CRMs that submit results will be archived. It is intended that

these fields can be downloaded and used (e.g., for work on improving GCM parameterizations) whether or not researchers choose to run their own CRM simulations of this case study. Second, the data analyses performed for this study (e.g., mean profiles during the six days of active monsoon, six days of suppressed monsoon, and 24-hour sub-periods) will also be archived. It is intended that the TWP-ICE case study may then be used more readily as a benchmark for future model development and evaluation. Model results and analyzed data will be archived at the ARM Climate Research Facility.

6. References

Allen, G., G. Vaughan, K. N. Bower, P. I. Williams, J. Crosier, M. Flynn, P. Connolly, J. F. Hamilton, J. D. Lee, J. E. Saxton, N. M. Watson, M. Gallagher, H. Coe, J. Allan, T. W. Choularton, and A. C. Lewis, 2008: Aerosol and trace gas measurements in the Darwin area during the wet season, *JGR*, *113*, D06306, doi:10.1029/2007JD008706.

Barth, M.C., S.-W. Kim, C. Wang, K.E. Pickering, L.E. Ott, G. Stenchikov, M. Leriche, S. Cautenet, J.-P. Pinty, C. Barthe, C. Mari, J. Helsdon, R. Farley, A.M. Fridlind, A.S. Ackerman, V. Spiridonov, and B. Telenta, 2007: Cloud-scale model intercomparison of chemical constituent transport in deep convection, *Atmos. Chem. Phys., 7*, 4709-4731.

Gettelman, A. and P. M. de F. Forster, 2002: A climatology of the tropical tropopause layer, *J. Meteorol. Soc. Japan*, *80*, 911–924.

Horváth, A., and B. J. Soden, 2008: Lagrangian diagnostics of tropical deep convection and its effect upon upper-tropospheric humidity, *J. Clim., 21,* 1013–1028.

Li, X., C.-H. Sui, and K.-M. Lau, 2002: Precipitation efficiency in the tropical convective regime: A 2-D cloud resolving modeling study, *J. Meteorol. Soc. Japan, 80*, 205–212.

May, P. T., J. H. Mather, G. Vaughan, and C. Jakob, 2008: Characterizing oceanic convective cloud systems—The Tropical Warm Pool International Cloud Experiment, *Bull. Am. Meteorol. Soc.*, *154*, 153-155, doi:10.1175/BAMS-89-2-153.

Randall, D.A., R.A. Wood, S. Bony, R. Colman, T. Fichefet, J. Fyfe, V. Kattsov, A. Pitman, J. Shukla, J. Srinivasan, R.J. Stouffer, A. Sumi and K.E. Taylor, 2007: Climate Models and Their Evaluation, In: *Climate Change 2007: The Physical Science Basis*. Contribution of Working Group I to the Fourth Assessment Report of the Intergovernmental Panel on Climate Change [Solomon, S., D. Qin, M. Manning, Z. Chen, M. Marquis, K.B. Averyt, M.Tignor and H.L. Miller (eds.)], Cambridge University Press, Cambridge, United Kingdom and New York, NY, USA.

Sherwood, S. C., and A. E. Dessler, 2001: A model for transport across the tropical tropopause, *J. Atmos. Sci., 58*, 765–779.

Vaughan, G., C. Schiller, A. R. MacKenzie, K. N. Bower, T. Peter, H. Schlager, N. R. P. Harris, and P. T. May, 2008: Studies in a natural laboratory: High-altitude aircraft measurements around deep tropical convection, *Bull. Am. Meteorol. Soc.*, in press.